Surface Temperature Control in Plasma Deposition of Metal Matrix Composites

S. Koskie*, S. C. Shah†, E. S. Russell‡

* Princeton University, Princeton, NJ, † RelMan, Inc., Mountain View, CA, ‡ GE Aircraft Engines, Lynn, MA

Abstract This paper describes control of target surface temperature in the inductively coupled plasma deposition (ICPD) process used in manufacture of metal matrix composites. Temperature feedback is provided by an infrared camera; the DC plate current input to an RF power oscillator circuit is adjusted to maintain the desired surface temperature. The spray target is a cylindrical mandrel which translates and rotates beneath a stationary spray gun.

Because of the periodic translational and rotational motions of the mandrel, the linearised model relating the torch power to observed temperature is periodic time-varying. By holding the input constant over half the translation period and averaging the output over that time period, a nearly time-invariant linear model of the process is obtained. A logic-based signal processing algorithm removes the spurious and irrelevant measurements and averages valid measurements over a single deposition pass. System identification on the processed input-output data produced models in innovations form. The identified models and model uncertainty estimates were used to design a controller for spatially averaged substrate or deposit temperature. A frequency-weighted LQG controller design augments the plant with two integrators, in order to allow the controller to track a ramp reference command with zero steady-state error. Worst-case analysis of tracking performance based on the model uncertainty bounds gave a robust controller as well as insight into limitations due to model uncertainty. A workstation-based rapid prototyping system that included an i386 real-time controller was used to acquire data, identify models, and perform analysis and design. Real-time implementation of the algorithms was facilitated by a C language source code generator and interactive real-time displays on the workstation monitor. The resulting controller communicated with the facility's conventional programmable controller and included an interactive operator interface taking input from both the mouse and keyboard. Using scripts to perform analysis and design functions, the complete development cycle, including system identification, control design, and robustness analysis, and re-implementation takes on the order of several hours to repeat in the event of changes in process equipment or configuration.

Keywords temperature control of deposit, metal matrix composite monotape, system identification, robust control, rapid prototyping.

1 Introduction

Metal matrix composites (MMCs) for aerospace structures are currently being manufactured using inductively coupled plasma enhanced deposition (ICPD) [Siemers and Jackson, 1990]. In this process, a plasma torch is used to deposit a spray of molten metal droplets onto continuous ceramic fibers. ICPD process consistency can be greatly enhanced by improved temperature control. In particular, the control of surface temperature can help in controlling droplet adherence, fiber damage, monotape curvature, and residual stresses in the fiber and deposit.

The ICPD equipment, shown in Figure 1, consists of a vacuum chamber fitted with an induction plasma gun, which generates a spray of molten droplets, and a shaft, which can rotate and translate the deposit target. During preheat, the mandrel is first heated by the torch to an initial temperature without the metal droplets. Deposition begins when powder metal is fed through the gun centerline at a controlled rate. The powder particles are melted by the plasma, then rapidly solidify as they impinge on the fiber-wound mandrel.

In contrast to traditional control approaches that deal with improving control performance for a given prior model, we focus on both improving the models from experimental data and improving the resulting control. Understanding how model structures and the associated computational procedures place demands on various design, analysis and implementation resources allows efficient navigation through the design space [Shah *et al.*, 1991].

1.1 Control Objectives

From earlier research it was determined that accurate control of surface temperature during deposition would greatly improve process consistency and material quality [Backman *et al.*, 1990]. An infrared camera looking at the translating mandrel provides temperature feedback. The DC plate current input to the RF oscillator circuit is adjusted to maintain the desired surface temperature. Because of the translation and rotation of the mandrel, the temperature signal from the stationary infrared camera occasionally contains meaningless values from regions beyond the target as the target translates out of the field of view. Anomalous surface features may also result in spurious temperature readings.

The main challenge in achieving the control objectives lay in dealing with a very noisy temperature signal, using the signal to identify a model and using it to control the process.

1.2 Model Structure

The ICPD control objective was the control of deposition surface temperature through plate current actuation. The motion of the mandrel relative to the torch causes very large periodic variations in temperature at any specific location on the infrared camera image. Slower variations in temperature, due to changes in torch power, are super-imposed on this large variation. By holding the torch input constant over each stroke and averaging the temperature measurement over the stroke, we created an approximate time-invariant description of the time varying system. This is similar to the so-called lifting transformation of multi-rate systems.

Given the level of noise in the measurements, we chose to model and identify the noise along with the plant dynamics, then use the identified noise dynamics in constructing a time-invariant Kalman Filter. The model in innovations form [Kailath, 1968] is a convenient parameterisation for performing these computations.

2 System Identification Experiments

2.1 Experiment Design

The range of frequencies of interest selected for the system identification effort was 0 to 0.1 Hz. We chose the upper limit of the frequency band to be ten times the estimated plant bandwidth so as to reduce model

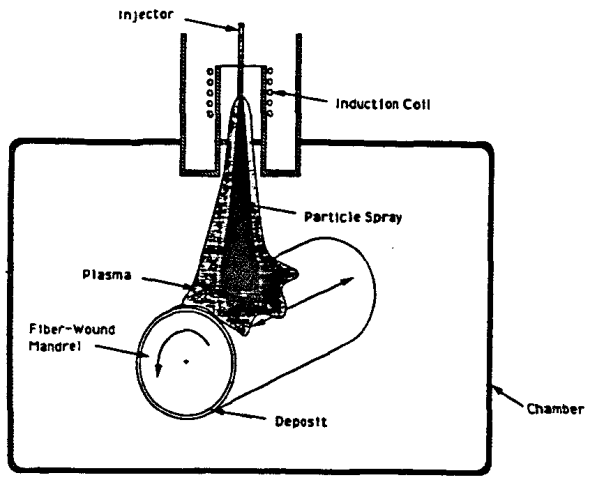

Figure 1: The plasma spray facility

uncertainty just outside the open-loop plant bandwidth. The reduced uncertainty also allows us to increase the closed loop bandwidth beyond the open-loop bandwidth. We chose an operating point and observed perturbations about that operating point to compute a model and to verify its accuracy in the region of interest. We tested two excitation amplitudes at the nominal plate current operating point, as well as a single amplitude at one operating point above and one below the nominal plate current. We chose a PseudoRandom Binary Sequence (PRBS) [Davies, 1966] input signal for whiteness of frequency content in the range of interest.

We selected a unit sampling interval corresponding to the stroke length for the PRBS signal. A sampling interval of 16 s was used for the tests in which the stroke length was 8 inches and 16.2 s was used for a stroke length of 8.1 inches.

2.2 Data Analysis

The processed plate current and surface temperature signals for the nominal operating point data set are shown in Figure 2.

2.3 Procedure

The system identification procedure described here was chosen for computational tractability. In contrast to maximum likelihood estimation of ARMAX parameters or other methods leading to nonconvex optimization, the procedure we chose decomposes the identification problem into two convex optimization problems. Each of these problems has a unique minimum, whereas nonconvex problems require initial estimates that are very close to the actual values in order to find the global minimum rather than a local minimum. In our experience, local minima often produce very poor models if the underlying optimization is nonconvex. In the first step of our procedure we developed a plant model. Then from the output error, we computed a model of the noise process.

For the plant model, we chose a transfer function form: AutoRegressive with eXogenous inputs (ARX). The noise model structure we chose was an AutoRegressive (AR) structure. Using the ARX and AR models, the prediction error is a quadratic function of the data vectors and is convex in the estimation parameters. This means that the prediction error has a unique minimum. We verified that the prediction errors of the AR model were uncorrelated.

Because model bias decreases with increasing model order in an ARX structure, we first fit high order models to minimize bias, and then performed a model reduction step in which we computed a low order model whose behavior in the frequency range of interest closely matched that of the high order model. We then verified that frequency and step responses of the two models were closely matched at DC and in the frequency range of interest. Finally, we verified that the system behavior over the range of operating conditions of interest was sufficiently linear.

2.3.1 High Order Model Computation Using Least Squares

In this step, we obtained a model of sufficiently high order so that little improvement in data fitting was seen by increasing the order. Higher order terms are used in approximating the noise dynamics within the ARX structure that would otherwise seriously corrupt the effective plant transfer function estimate [Ljung, 1987].

The ARX model used for the plant was of the form

$$y_k + a_1 y_{k-1} + \cdots + a_{n_a} y_{k-n_a} = b_1 u_{k-1} + \cdots + b_{n_b} u_{k-n_b} + e_k \quad (1)$$

where the input is u, the output is y and the error term is e. No u_k term appears in this equation because, in controlling the plant, we can take into account only previous measurements in computing the current control command. A batch least squares fit was used to minimize the value of the sum of squared equation errors. The noise model was computed by fitting an autoregressive (AR) model to the output error, ϵ, which is equal to the difference between the measured plant output, y, and the computed output, $\hat{y}(t|\theta, u_{t-1}, u_{t-2}, \ldots)$, given the parameter vector θ and only the inputs u. The autoregressive model can be written as

$$\sum_{i=0}^{n_c} c_i \epsilon_{k-i} = 0 \quad (2)$$

Two methods were used for determining the order of the model to be fit with batch least squares. In the first, the error variance was plotted as a function of model order. An order high enough that the error as a function of order has leveled off was selected. This result was verified by computing frequency response magnitude over a range of frequencies using increasing model orders and determining the order at which the responses converged. Twentieth order was chosen for the high order models.

2.3.2 Frequency Weighted Least Squares Model Reduction

For computational tractability, a high order system model is undesirable. Luckily, the higher order model contains information that is not needed for control.

In order to simplify the model, we matched the behavior of the high order model only in the frequency region of interest. This was done by using the frequency weighted least squares procedure to fit a model of the form in Equation 1 to the system frequency response, expressed as a vector of complex magnitudes, $\hat{\mathbf{G}}_{20}$ and a vector of corresponding frequencies, Ω, both of length m. These vectors were computed by substituting $z_i = e^{j\omega_i}$ into the high order transfer function estimate, $\hat{\mathbf{G}}_{20}(z) = \hat{\mathbf{A}}_{20}(z)/\hat{\mathbf{B}}_{20}(z)$ for each ω_i in Ω. The low order transfer function estimate $\hat{\mathbf{G}}_1(z) = \hat{\mathbf{A}}_1(z)/\hat{\mathbf{B}}_1(z)$ was obtained by using batch least squares to minimize

$$\sum_{k=1}^{m} w_k |\hat{A}_1(e^{j\omega_k})\hat{G}_{20}(e^{j\omega_k}) - \hat{B}_1(e^{j\omega_k})|^2 \quad (3)$$

where w_k is the weight corresponding to the frequency ω_k. We used high weights in the low frequency regions is order to match the DC gain. The actual plant is unresponsive to inputs at frequencies above 0.1 Hz so low weights were selected to cause the fit to ignore high frequency behavior of the high order model. Typically the ratios of low to high frequency weights were 100:1. The model produced was thus in the form of numerator and denominator polynomials of a transfer function. A first order plant model gave a good frequency response fit to the high order plant model between 0 and 0.1 Hz.

2.4 Identified Model

The reduced order identified model is described mathematically in discrete state space form as

$$\mathbf{x}_{k+1} = A_c \mathbf{x}_k + B_c \mathbf{u}_k \quad (4)$$

$$y_k = C_c \mathbf{x}_k + D_c \mathbf{u}_k \quad (5)$$

where

$$\mathbf{x}_k = \begin{bmatrix} x_P \\ x_N \end{bmatrix} \quad \mathbf{u}_k = \begin{bmatrix} u_k \\ e_k \end{bmatrix} \quad (6)$$

In the above equations, x_{Pk} is the plant state, x_{Nk} is the noise state, y_k is the output, and u_k is the plant input, at time step k. The innovation sequence e_k, given by

$$e_k = y_k - \hat{y}_k \quad (7)$$

represents that part of the current input that cannot be predicted from previous data. The A_c, B_c, C_c, and D_c matrices are

$$A_c = \begin{bmatrix} A_P & 0 \\ 0 & A_N \end{bmatrix} \quad (8)$$

$$B_c = \begin{bmatrix} B_P & 0 \\ 0 & B_N \end{bmatrix} \quad (9)$$

$$C_c = \begin{bmatrix} C_P & C_N \end{bmatrix} \quad (10)$$

$$D_c = \begin{bmatrix} 0 & I \end{bmatrix} \quad (11)$$

$$(12)$$

where the subscript P refers to the plant model and the subscript N

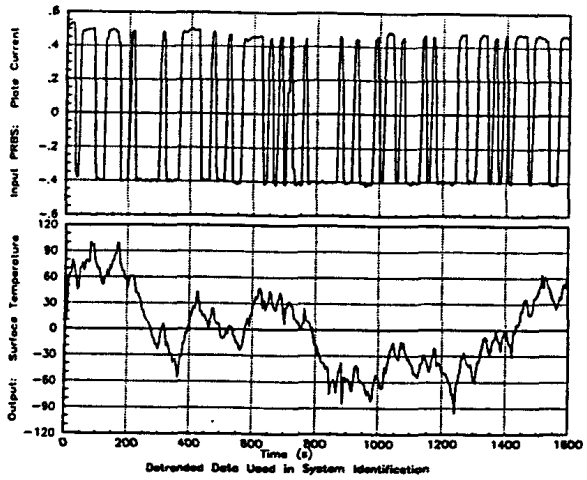

Figure 2: The plate current and spatially averaged deposit surface temperature

refers to the noise model. These matrices are determined in the system identification procedure described above.

2.4.1 Verification

The step response and frequency responses of the high and low order models were found to match well. Next, we examined the difference between the surface temperature data and the model output corresponding to the test input. As shown in Figure 3, the behavior of the plant model is a good approximation to that of the actual plant. To determine the range of plate currents over which the model is valid, we computed models for two other data sets and the eigenvalues compared. The plant model eigenvalues for the three cases were similar.

We verified that the innovations sequence computed using the Kalman filter for the reduced order plant showed that the innovation sequence was uncorrelated.

2.4.2 Model Uncertainty

For later steps in which we verified that the controller behavior on the plant would be acceptable, we needed a measure of the uncertainty associated with the system identification model. Model uncertainty can be described as an additive component Δ representing the difference between the actual system transfer function G and the transfer function estimate $\hat{G}$. As described by Kosut [Kosut, 1988], a useful method of describing the uncertainty associated with a model resulting from a system identification procedure is to estimate the non-parametric frequency domain transfer function. To obtain this estimate, the first step is to compute the output error

$$\eta_k = y_k - \hat{G}u_k = (G - \hat{G})u_k + d_k = \Delta u_k + d_k \qquad (13)$$

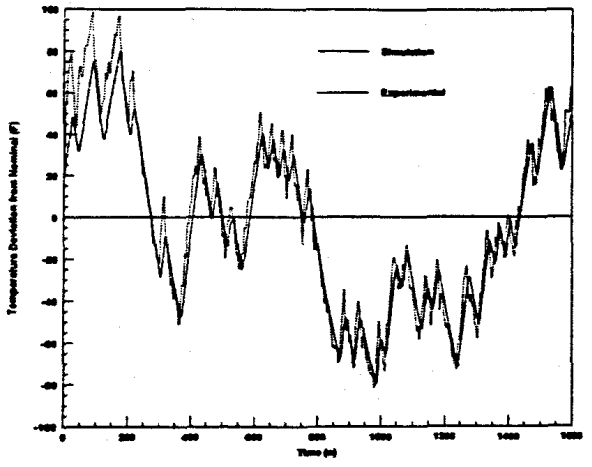

Figure 3: Comparison of the plant and identified plant model responses to the test input

Allocating all output errors to model uncertainty, a non-parametric frequency domain transfer function estimate for the additive uncertainty for the model $\hat{G}$ is

$$\Delta = \frac{\hat{S}_{\eta u}}{\hat{S}_{uu}} \qquad (14)$$

As the output error results from both noise and modelling error, the above approximation is conservative.

3 Control Design

We used the identified models and model uncertainty estimates to design a controller for spatially averaged substrate or deposit temperature. The controller used plate current actuation. The design procedure consists of three steps: estimator design, computation of controller gains, and design of switching logic for the transition from manual to automatic control.

3.1 Estimator Design

Because the optimal gain was estimated directly in the system identification process described earlier, no further computation is required. The estimator we used has been structured such that the updated state estimates are output directly.

3.2 Frequency-Shaped LQG Control Design

In order to achieve zero steady state error in following a ramp input, we augmented the plant model by adding two integrators. These added states have the effect of weighting low frequency errors more heavily than high frequency inputs.

The controller is shown in Figure 4. For testing, it is included in a higher level block which also contains the ramp command generator and the system model. Within the controller, the state space representations of the plant and noise models are combined into a single state space matrix, the estimator or Kalman filter, which is then augmented by a pair of integrators. The integrators allow the controller to follow a ramp input with zero steady state error. (Augmenting the plant with a single integrator would allow the controller to follow a step input with zero steady state error.) The control gains kx and ki are contained in blocks 25 and 15, respectively. The controller also contains logic for limiting the plate current to acceptable values, and switching logic for the transfer from manual to automatic control. This switching logic is described in more detail below.

3.3 Stability and Worst-Case Tracking Robustness Analysis

Worst-case analysis of tracking performance based on the model uncertainty bounds produced a robust controller as well as insight into limitations due to model uncertainty.

The controller design procedure described above computes control gains based on the nominal identified plant model. In reality, the behavior of the nominal plant will not exactly match that of the true plant. Before testing the controller behavior on the actual plant, we need to analyse the effects of the model uncertainty on closed loop stability and tracking performance. In the following analysis, we will use the model uncertainty estimate obtained in the system identification procedure. References for the procedures described below include [Boyd and Barratt, 1991], [Integrated Systems, 1991], [Maciejowski, 1989], [Morari and Zafiriou, 1989], and [ONR/Honeywell, 1984].

3.3.1 Stability Margin

The first step of our robustness analysis determines the margin of stability to additive model error. Additive model error is viewed as an additional transfer function in parallel with the nominal (identified) plant. The transfer function describing the behavior of the true plant can then be written as

$$P(j\omega) = P_n(j\omega) + \Delta_a(j\omega) \qquad (15)$$

A simplified block diagram, which uses this description of this plant was used in the robustness analysis.

The model uncertainty is isolated and the dynamics of the rest of the system are lumped into a single block corresponding to the nominal transfer function. This transfer function includes the effects of the nominal plant, the controller, and the estimator. The connection of the nominal and uncertain transfer functions becomes a simple feedback

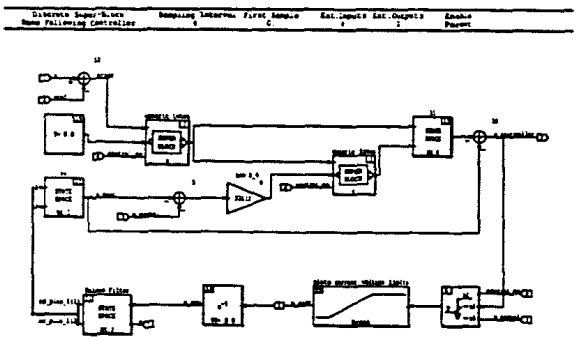

Figure 4: Block diagram of ramp following controller

connection. The equivalent transfer function from the reference signal to the output, which we will call H_{pert}, is

$$H_{pert} = \frac{H_{nom}}{I - \Delta_a H_{nom}} \tag{16}$$

To verify that the actual closed-loop controller implementation on the ICPD plant will be stable, we need to determine whether the perturbed plant transfer function, H_{pert} is stable for all possible values of Δ_a.

Following the derivation in [Boyd and Barratt, 1991], we described the system in matrix equation form as

$$\begin{bmatrix} y \\ u \end{bmatrix} = \begin{bmatrix} H_{yr} & H_{yd} \\ H_{ur} & H_{ud} \end{bmatrix} \begin{bmatrix} r \\ d \end{bmatrix} \tag{17}$$

where r, u, d, and y are the reference input, control effort, plant output due to the additive uncertainty term, and plant output, respectively. Each element H_{ij} of the above matrix represents the transfer function from input j to output i.

The small gain theorem [Boyd and Barratt, 1991], applied to the equivalent transfer function, H_{pert}, states that the system is stable if

$$|H_{ud}(j\omega)||\Delta_a(j\omega)| < 1, \quad \forall\omega \tag{18}$$

That is, the system is robustly stable if the product of the gain of the transfer function H_{ud} and the magnitude of the additive uncertainty is less than 1. The inequality in Equation 18 can be expressed in the following form:

$$20\log|H_{ud}(j\omega)| + 20\log|\Delta_a(j\omega)| < 0 \tag{19}$$

from which, the maximum allowable uncertainty bound (Δ_{am}) for closed loop stability of the system can be expressed as:

$$20\log|\Delta_{am}| = -20\log|H_{ud}| \tag{20}$$

As shown in Figure 5, the model uncertainty estimated as part of the system identification procedure was within the maximum allowable model uncertainty for all frequencies between 0.002 and 0.2. As the uncertainty estimate is conservative, tending to overestimate rather than underestimate the actual error, this indicates that the LQG controller is robustly stable.

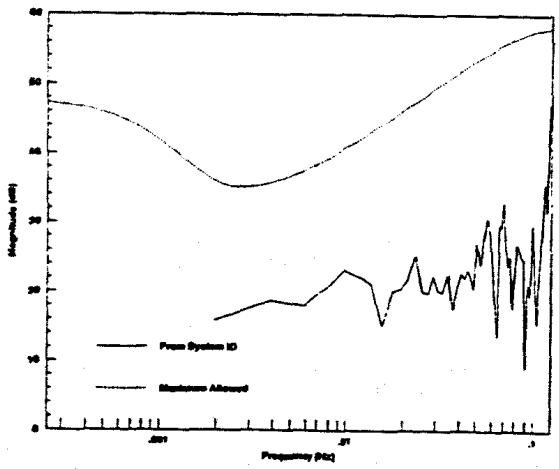

Figure 5: Comparison of uncertainty estimated in system ID procedure with maximum allowable uncertainty for robust stability

3.3.2 Worst-Case Performance Analysis

Model uncertainty affects not only the robustness, but also the performance of a feedback system. To address this issue, we examined the worst-case tracking performance of the LQG controller in response to perturbations about the nominal plant.

Obtaining the worst-case performance of the controller, consists of solving the following optimisation problem:

$$G_{WC}(\omega) = \max_{\Delta_a}\{|H_{pert}(j\omega, \Delta_a)| \text{ such that } \Delta_a \leq U(j\omega)\} \tag{21}$$

where $U(j\omega)$ is an upper bound on the uncertainty magnitude as determined from the system identification analysis.

The optimisation problem posed in Equation 21 was solved using the WCBODE routine [Milletti and Kosut, 1989] of MATRIX$_X$ to analyze the performance from the input r to the output error e. This worst case analysis compares the nominal tracking performance with the worst-case tracking performance. The comparison of the nominal and the worst-case tracking performance showed that to reduce the tracking error around 0.002Hz, we should improve the model in that frequency region. This can be achieved by increasing the excitation signal strength in that region during subsequent system identification experiments.

3.4 Bumpless Transfer Logic

One means of reducing the transient response just after switchover to a standard LQG controller is to allow the state estimation errors to become small before initiating the switchover. However, in the above controller design, the values of the integrator states do not correspond to measurable physical states. If the automatic controller were in control from the time the system were started, the initial values of these states might be known. As they are not, a mechanism for initialising the integrator states is required in order to facilitate transfer from manual to automatic control. Our controller accomplishes this by driving the state of the first integrator to zero and the state of the second to the value of manual current command divided by the corresponding state gain. After verifying that the controller output is tracking the manual command, the system allows the operator to make the transfer.

4 Implementation of the Ramp-following Controller

A workstation-based rapid prototyping system which included an i386-based real-time controller was used to acquire data, identify models, and perform analysis and design. Real-time implementation of the algorithms was facilitated by a C language source code generator [Lehman *et al.*, 1989] and interactive real-time displays on the workstation monitor. The resulting controller communicated with the facility's conventional programmable controller via analog signals and included an interactive operator interface taking input from both the mouse and keyboard. Using scripts to perform analysis and design functions, the complete development cycle, including system identification, control design, and robustness analysis, takes on the order several hours to repeat in the event of changes in process equipment or configuration.

The prototype controller described above was tested on the ICPD facility on several occasions. The steps involved in running the controller include generating, compiling, and linking C-language source code, (required only if changes are made to the block diagram,) downloading to the i386 processor, and starting the controller. Recorded commanded and spatially averaged measured temperatures are shown in Figure 6.

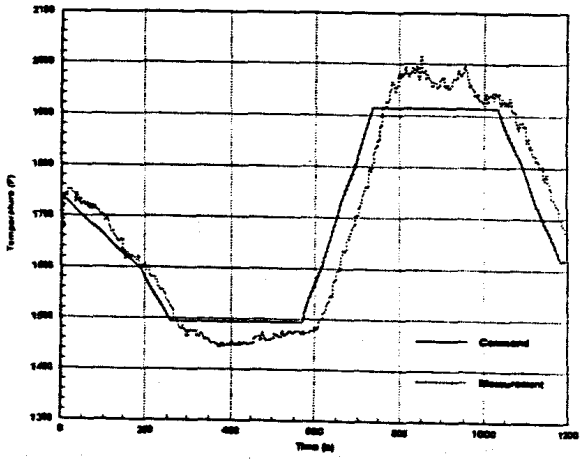

Figure 6: Experimental data from a test of the ramp following controller

5 Conclusions and Recommendations

Based on past research on the plasma enhanced deposition process, we selected deposition temperature as a critical process parameter in reducing product quality variations.

The results reported here are promising in demonstrating a controller based on input-output data from in-situ temperature measurements in a plasma enhanced deposition process. It remains to be verified that better control of deposition temperature has, in fact, resulted in a more repeatable product quality.

The initial iteration through the control design cycle showed how model uncertainty affected controller performance. Subsequent model refinement iterations can utilise this information in design of experiments. Further experiments would enable us to better understand model variation with operating point.

6 Acknowledgements

This work was performed as a subcontract under the DARPA/ONR Intelligent Processing of Materials — Metal Matrix Composites (IPM - MMC) contract, N00014-90-C-0060, with GE Aircraft Engines (GE–AE) in Lynn, MA.

Dan Backman at GE–AE and Henk Aling at Integrated Systems, Inc. (ISI) in Santa Clara, CA, made major contributions to the work presented here. The first two authors were with ISI at the time this work was performed.

7 References

Backman, D. G., *et al.* (1990). Intelligent Processing for Metal Matrix Composites. In H. N. G. Wadley and W. E. Eckhart, Jr., (Eds.), *Intelligent Processing of Materials.* The Minerals, Metals, and Materials Society.

Boyd, S. P. and C. H. Barratt (1991). *Linear Control Design: Limits of Performance.* Prentice-Hall, Englewood Cliffs, NJ.

Davies, W. D. T. (1966). Generation and Properties of Maximum-Length Sequences. Parts 1, 2, and 3. *Control,* June, July, and August 1966.

Doyle, J. (1984). Lecture Notes. ONR/Honeywell Workshop on Advances in Multivariable Control, Minneapolis, MN.

Integrated Systems, Inc. (1991). *$MATRIX_x$ Robust Control Module (Documentation).* Integrated Systems, Inc., Santa Clara, CA.

Kailath, T. (1968). An Innovations Approach to Least-Squares Estimation Part I: Linear Filtering in Additive White Noise. *IEEE Transactions on Automatic Control,* AC-13(6), 646-655.

Ljung, L. (1987). *System Identification: Theory for the User.* Prentice-Hall, Englewood Cliffs, NJ.

Kosut, R. L. (1988). Adaptive Control of Large Space Structures: Uncertainty Estimation and Robust Control Calibration. In S. N. Atluri and A. K. Amos (Eds.) *Large Space Structures: Dynamics and Control.* Springer Verlag, Berlin.

Lehman, L., S. C. Shah, and D. Varvell. (1989) Multirate Real Time Control System Code Generator, U. S. Patent No. 4,796,179.

Maciejowski, J. M. (1989). *Multivariable Feedback Design.* Addison-Wesley, New York.

Milletti, U. and R. L. Kosut (1989). Robust Control Design and Analysis for a Flexible Space Structure: Robust Control Module Application Note. Integrated Systems, Inc., Santa Clara, CA.

M. Morari and E. Zafiriou. (1989). *Robust Process Control.* Prentice-Hall, Engelwood Cliffs, NJ.

Shah, S. C., *et al.* (1992). A Methodology for Intelligent Control of Manufacturing Processes. In E. F. Matthys and B. Kushner (Eds.), *Advanced Sensing, Modeling, and Control of Materials Processing.* The Minerals, Metals, and Materials Society.

Siemers P. A. and Jackson J. J. (1990). Ti_3Al/SCS – 6 MMC Fabrication by Induction Plasma Deposition. Titanium Aluminide Composite Workshop, Orlando, FL.